Architecture of a self-fragmenting droplets cascade

Gautier Verhille [1,*] Chihiro Inoue [2,†] and Emmanuel Villermaux [1,3,‡]

[1]*Aix Marseille Université, CNRS, and Centrale Marseille, IRPHE Marseille, Marseille, France*
[2]*Kyushu University, Department of Aeronautics and Astronautics, Fukuoka, Japan*
[3]*Institut Universitaire de France, Paris, France*

We report quantitative imaging experiments describing the three-dimensional (3D) bursting cascade of droplets from a liquid melt reacting with the oxygen of air which explode sequentially to produce ever smaller fragments. The 3D space-time resolved trajectories of the fragmenting drops reveal an arborescent structure of branchings defining the cascade steps, each random in direction and shortening along the cascade, in a way we determine. The phenomenon is a unique and prototypical illustration of the so-called Richardson regime, namely, an accelerated cascade towards smaller scales. The phenomenon, which coincides with the early time dispersion period of a Brownian motion, featuring here ever shrinking steps, is well captured by a Langevin dynamics.

The notion of cascade is a convenient mental image to represent the dynamics of a number of phenomena. For instance, the direct cascade of energy and enstrophy fluxes towards dissipative scales or the inverse cascade of energy are well-know paradigms in fluid turbulence [1–4]. It is, also, sometimes an explicitly observable physical reality as in viscous filaments undergoing an iterated fission cascade of capillary instabilities [5], or for rough liquid ligaments breaking up after an inverse cascade of aggregations, not to mention size-reduction of solids by sequential crushing and grinding [6] (see Ref. [7] for a critical review about cascades in fragmentation phenomena). Here, a three-dimensional (3D) cascade is obtained by firing a *Senkou-Hanabi*, a traditional hand-held firework known since the Edo period (1603-1868) in Japan. It consists of light streaks similar to branched pine needles, with ever smaller ramifications. These streaks are the trajectories of incandescent reactive liquid droplets bursting from a melted powder (so-called "black powder," a mixture of carbon, C; sulfur, S; and potassium nitrate, KNO_3). Inoue et al. [8] have uncovered the detailed sequence of events, which involve a chemical reaction with the oxygen of air, thermal decomposition of metastable compounds in the melt, gas bubble nucleation and bursting, and formation of liquid ligaments and droplets, all this occurring in a sequential fashion proceeding over many generations. Like in atom fission [9], droplets divide sequentially and self-similarly, down to an elementary brick; the cascade ends when heat losses overcome chemical heat release, quenching the reaction.

Using an original high-speed 3D tracking method, we reconstruct the trajectories of the drops to investigate the nature of the cascade arborescence which results from the randomness of the nucleation sites in each drop. This unique underlying dynamics offers the opportunity to address a number of fundamental paradigms like Brownian motion with shrinking steps [10,11] and the concrete realization of an accelerated Richardson cascade [12], for example.

The trajectories are measured using three non-coplanar synchronized *Phantom* fast cameras. The firework arborescence is probed using the convex hull volume method [13,14] where the reconstructed volume is discretized in voxels, with only those detected by the three cameras simultaneously being stored. Two sets of experiments are presented (Fig. 1). In the first, the bursting dynamics of individual drops is investigated with a total reconstruction volume of the order of 1 cm^3 and a resolution (the voxel size) of 30 μm. The second, which is intended to measure the global architecture of the cascade, has a reconstruction volume of the order of 125 cm^3 and a resolution of 150 μm.

At each cascade step, a mother drop containing C reacts with the O_2 of air through a strongly exothermic reaction, heating the liquid which nucleates gas cavities of endothermically decomposing, volatile substances and bursts (see Ref. [8] and Fig. 1). The process repeats sequentially with the typical time between two bursting events given by the drop heating time:

$$\tau_n \sim R_n^2/\kappa \tag{1}$$
$$= \tau_0 \beta^{2n}, \quad \text{with} \quad R_n = \beta R_{n-1} = R_0 \beta^n, \tag{2}$$

where R_n is the radius of the drop at step n and κ is the thermal diffusivity of the molten mixture. This interbursting time is the time interval between the appearance of the drop at the nth generation and its division into daughter droplets at generation $n + 1$. The cascade is self-similar for a constant size reduction factor of $\beta < 1$, for which the interbursting time τ_n decreases exponentially [Eq. (2) and Fig. 2(b)].

Between two bursts, the drop evolves mainly ballistically modulo an evanescent viscous damping correction discussed later, as shown on the reconstructed trajectory in Fig. 1. At a

*gautier.verhille@irphe.univ-mrs.fr
†inoue.chihiro@aero.kyushu-u.ac.jp
‡emmanuel.villermaux@univ-amu.fr
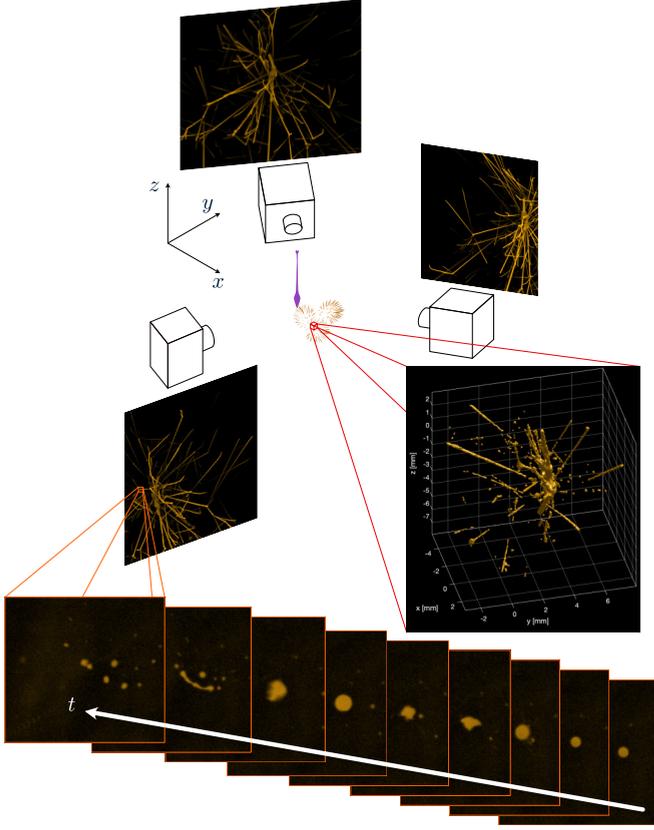
FIG. 1. The 3D reconstruction of the trajectories' arborescence of bursting drops in a firework, obtained from regularly spaced snapshots of three non-coplanar, synchronized, high-speed cameras (see movie in Supplemental Material [15]).

FIG. 2. (a) Drop trajectory from the 3D reconstruction featuring $n = 6$ steps (left) and from a $1/25$ s exposure picture, where the mother *Senkou-Hanabi* drop is visible (right). (b) Bursting time τ_n; the red line is from Eq. (2) with $\beta = 0.9$. (c) Mean squared velocity $\langle V^2 \rangle$ through the cascade; the red line is from Eq. (11). (d) Distribution of the velocity $\mathcal{P}(V)$ averaged over the entire cascade; the dashed line is from Eq. (20) and the solid red line is from Eq. (21). (e) Mean squared drop position $\langle R^2 \rangle$ versus cascade step n; the red line is from Eq. (16) and the dashed line is $\sim n^3$.

bursting event, mass and impulse conservation are such that

$$MV = \left(M - \sum_i m_i\right)V' + \sum_i m_i \boldsymbol{v}_i, \qquad (3)$$

where M and V are the mass and the velocity of the mother drop before burst, V' is its velocity after, and m_i and $\boldsymbol{v}_i$ are the masses and velocities of the i (a few units) ejected daughter drops. The ejection of drops results in a force, $\boldsymbol{f}$, communicated to the mother drop:

$$\boldsymbol{f} = \frac{m\boldsymbol{v}}{\Delta t}, \qquad (4)$$

where $m\boldsymbol{v} = \sum_i m_i \boldsymbol{v}_i$ and $\Delta t \sim \sqrt{\rho R_n^3/\sigma}$ is the (short compared to τ_n, see Ref. [8]) duration of a bursting event, with ρ and σ being the density and surface tension of the melt, respectively. This force is responsible for diverting the drop from its rectilinear trajectory, which is intermittently reoriented, at a mean pace given by τ_n. As seen in Fig. 2(a), the sizes of the daughter drops are usually much smaller than the size of the mother drop, so that $\sum_i m_i/M \ll 1$, this fraction being constant along the cascade [8]. Denoting $\Delta V = V' - V$ the mother drop velocity change, we thus have approximately

$$\Delta V \approx \frac{m}{M} \boldsymbol{v} \lesssim \boldsymbol{v}. \qquad (5)$$

Before we proceed with the consequences of this local dynamics on the fate of a mother drop in the firework arborescence, we need to wonder about the isotropy of the ejection process.

The ejection direction of the daughter drops [Fig. 3(a)] has an angle, θ, defined by $\boldsymbol{V} \cdot \boldsymbol{v}_i = V v_i \cos\theta$. If the emission of the daughter drops is isotropic, the probability distribution function (pdf) of the angle θ should be such that $\mathcal{P}_{\text{iso}}d\theta$ is the ratio of the solid angle $2\pi \sin\theta d\theta$ to the solid angle of the sphere 4π [16]; that is,

$$\mathcal{P}_{\text{iso}} = \tfrac{1}{2} \sin\theta. \qquad (6)$$

This relation slightly underestimates the probability of small angles $\theta < \pi/2$, the actual distribution being more skewed [Fig. 3(b)]. A possible reason for this asymmetry is that the nucleation of gas bubbles in a mother drop occurs preferentially at the front of the drop, in its forward direction. Bubbles
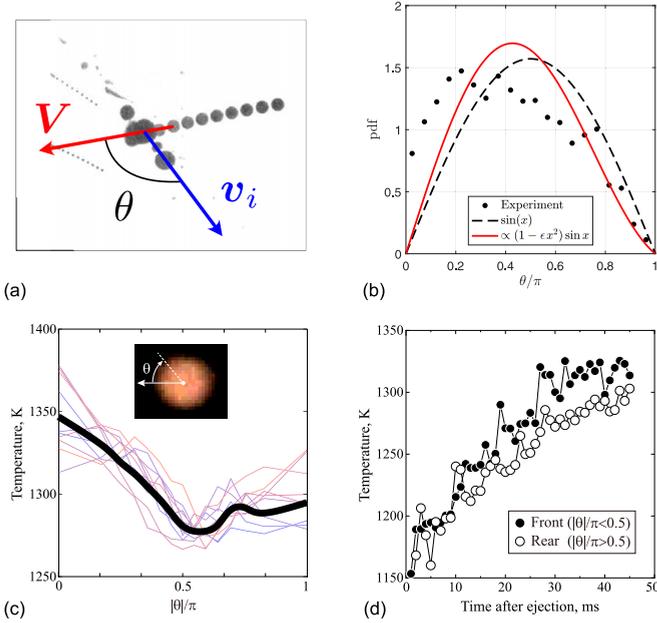
FIG. 3. (a) Measurement definition of the ejection angle θ between a mother drop and its daughter at burst. (b) Distribution of the angle θ; red line is from Eq. (7) with $\epsilon = 0.7$ and the dashed line is from Eq. (6). (c) In-flight drop surface temperature measured by two-color pyrometry [8] averaged over many drops 35 ms after ejection, showing the rear ($\theta = \pi$) and front ($\theta = 0$) asymmetry. (d) Drop temperature as a function of time illustrating the gradual increase between front and rear temperatures.

nucleate faster in the hottest regions of the drop and the oxygen flux feeding the exothermic reaction is higher in the region around the drop where the boundary layer is thinner, hastening there the diffusion-limited reaction [8]. Measurements of the surface temperature of flying droplets indeed show a slight but clear asymmetry in temperature of about 20 K higher at the front of the drop compared to the rear, superimposed on a global increase as the drop heats up [Figs. 3(c) and 3(d)].

This temperature difference can be explained thanks to the 3D reconstruction. Indeed, the Reynolds number $\text{Re} = VR/\nu$, with $R \sim 50\,\mu\text{m}$ being a typical drop radius measured in Inoue et al. [8], $V \sim 1$ m/s its typical speed, as shown in Fig. 2, and $\nu \sim 10^{-5}$ m^2/s the kinematic viscosity of air, is of the order of $\text{Re} \sim 5$. Because symmetry is broken by the drop translation, the kinematic boundary layer thickness, whose order of magnitude is $\delta_0 \sim \sqrt{\nu R/V}$, has an angular dependence of $\delta \approx \delta_0(1 + \epsilon\,\theta^2)$, making it thinner at the drop front (see, e.g., Ref. [17]). Since the oxygen flux is inversely proportional to δ, it is higher at the front than at the rear, thus explaining the temperature difference which induces more frequent ejections at the front, that is, for small θ. We may thus expect

$$\mathcal{P}_{\text{skew}} \propto (1 - \epsilon\,\theta^2)\sin\theta, \tag{7}$$

in qualitative agreement with the measured distribution, as seen in Fig. 3(b). Similar symmetry breakings have been identified in chemistry [18] and in the Marangoni stresses directed motion of droplets [19,20].

Having quantified the ejection isotropy bias which is noticeably, weak, we proceed further with the caricature of the

drop motion in Eq. (5) by considering a limit where $\boldsymbol{v}$ is a random variable with zero mean, thus reflecting isotropy. In this simple model, the drop experiences a velocity increment given by Eq. (5) at each step n of the cascade, each being independent of the others so that, up to constant factors,

$$\frac{d\boldsymbol{V}}{dn} = \boldsymbol{v}, \tag{8}$$

$$\langle \boldsymbol{v} \rangle = 0, \quad \text{and} \quad \langle \boldsymbol{v}_n \cdot \boldsymbol{v}_m \rangle = v_n^2\,\delta(n-m), \tag{9}$$

$$\text{with} \quad v_n^2 \sim \sigma/\rho R_n, \tag{10}$$

where $\delta(.)$ denotes the Dirac delta function, and v_n is the mean amplitude of the daughter drop ejection velocity [8] with radius R_n given in Eq. (2). The random velocity $\boldsymbol{v}$ is the analog of a "Langevin force" [21], whose correlation intensity increases here, by contrast with standard Brownian processes, along the cascade. The above system solves in

$$\langle \boldsymbol{V} \rangle = 0 \quad \text{and} \quad \langle \boldsymbol{V}^2 \rangle \sim 2v_0^2(\beta^{-n} - 1), \tag{11}$$

meaning that the drop velocity first diffuses $\langle \boldsymbol{V}^2 \rangle \sim 2v_0^2 n$ along n for $-n\ln\beta \ll 1$ (the mean translation is obviously zero) and then increases exponentially as $\langle \boldsymbol{V}^2 \rangle \sim 2v_0^2\beta^{-n}$ for $-n\ln\beta \gg 1$, both trends being not incompatible with those reported in Fig. 2(c), with β given by the evolution of the interbursting time. As the step number n increases, the amplitude of the drop velocity diverges, while its exploration radius $\boldsymbol{R}$ remains finite: These hand-held fireworks are localized "balls" with a finite radius (~ 5 cm) even if made of a very large number of uncorrelated ever finer segments [8] because the drop change of direction is increasingly frequent as the interbursting time decreases. In this respect, they represent an ideal random walk [10] with shrinking steps [11]. The limited resolution of the camera prevents an accurate measurement of the whole trajectories; the measurements are made in a localized subvolume in the frame of the first drop entering this volume, named the mother drop. The drop position is ruled by

$$\frac{d\boldsymbol{R}}{dt} = \boldsymbol{V}, \tag{12}$$

with t being the current time which is related to the cascade step n by

$$t = \sum_{i=0}^{n-1} \tau_i = \tau_0 \sum_{i=0}^{n-1} \beta^{2i} \sim \tau_0(1 - \beta^{2n}), \tag{13}$$

emphasizing the acceleration of the cascade since $dt/dn \sim \tau_0\beta^{2n}$ decays with n. We thus have

$$\boldsymbol{R} = 2\tau_0 \int_0^n \boldsymbol{V}(n')\beta^{2n'} dn', \tag{14}$$

with $\langle \boldsymbol{R} \rangle = 0$ since $\langle \boldsymbol{V} \rangle = 0$: The arborescence expands, but does not translate. The squared exploration radius

$$\langle \boldsymbol{R}^2 \rangle = 8\tau_0^2 \int_0^n dn' \int_0^{n'} dn'' \langle \boldsymbol{V}_{n'} \cdot \boldsymbol{V}_{n''} \rangle \beta^{n'+n''} \tag{15}$$

derives from an integration [22] of the velocity correlation function $\langle \boldsymbol{V}_{n'} \cdot \boldsymbol{V}_{m'} \rangle \sim 2v_0^2(\beta^{-n} - 1)$, leading to

$$\langle \boldsymbol{R}^2 \rangle \sim \frac{(v_0\tau_0)^2}{3}\beta^{4n}(\beta^{-n} - 1)^3(3 + 5\beta^{-n}), \tag{16}$$

a relation again in relatively good agreement with our measurements in law and absolute value. As expected, the exploration radius has a finite limit of $\langle \mathbf{R}^2 \rangle \sim (v_0 \tau_0)^2/3$ at infinite cascade steps ($-n \ln \beta \gg 1$) despite the velocity divergence, but more interestingly, its early steps behavior ($-n \ln \beta \ll 1$) displays a superballistic dependence since we have $\langle \mathbf{R}^2 \rangle \sim (-n \ln \beta)^3$. This $\langle \mathbf{R}^2 \rangle \sim n^3$ regime [see Fig. 2(e)] is called, in turbulence, the "Richardson regime" [12] and is a signature of the early time (here, small step number n), diffusive type of correlation of the velocity (i.e., $\langle V^2 \rangle \sim n$, see also Ref. [23] for a more involved formulation and Ref. [24] for a different context). As such, it is not particular to turbulence since it has been witnessed in standard Brownian motion [25], and is well known to be a feature of the Langevin model for an initially zero (like in the present problem) particle velocity [22,26,27]. It is nevertheless remarkable that, in the present variant of active Brownian motion [28–30], a feature routinely associated with high Reynolds number turbulence, or colloidal particles, is here observed in a mesoscopic object involving neither external stirring [31] nor thermal noise.

Interestingly, viscous drag from the outside air is subdominant, and its relative strength is not reinforced as the drops get smaller, lighter (mass $M_n \sim \rho R_n^3$), and faster. Adding a Stokes linear drag force of $-\alpha_n V$ from air with $\alpha_n = 6\pi \eta_a R_n$ (air viscosity η_a) in Eq. (17) leads to

$$\frac{d\mathbf{V}}{dn} = \mathbf{v} - \frac{\mathbf{V}}{N}, \tag{17}$$

$$\text{with} \quad N = \frac{M_n}{\alpha_n (dt/dn)} \sim \frac{\rho}{\rho_a} \frac{\kappa}{\nu_a}. \tag{18}$$

The factor N is constant, independent of n, and with $\kappa \sim 10^{-6}$ m^2/s and $\nu_a = \eta_a/\rho_a \sim 10^{-5}$ m^2/s, we have $N = O(10^2) \gg 1$. Air drag is always negligible; however, viscous dissipation does occur during the ejection stage, since the mother drop deforms considerably to release a ligament (see Fig. 1). The corresponding viscous dissipation time R_n^2/ν where ν is now the viscosity of the melt becomes shorter than the capillary ejection time $\Delta t \sim \sqrt{\rho R_n^3/\sigma}$ above for

$$n_\star \sim \ln\left(\frac{\sigma R_0}{\rho \nu^2}\right) \Big/ \ln \frac{1}{\beta}. \tag{19}$$

These melts are known to be appreciably viscous and cohesive ($\eta \approx 10^{-2}$ Pa s, $\sigma \approx 0.1$ N/m, see [32,33]), giving $n_\star \approx 10$ for binary fission ($\beta = 0.5$) and $n_\star \approx 65$ for $\beta = 0.9$ (Fig. 2), a threshold never met in the present case, the cascade being interrupted earlier at $n_c = O(10)$ by chemical quenching [8].

Access to a multiplicity of drops trajectories in the firework allows for the study of distributions, a natural aspect of a complete physical description [34]. Droplets are too small for our measurement technique to document their sizes, and the number of individual drop trajectories is not numerous enough to study statistics within single trajectories. However, ensemble averages, accumulating over the whole set of trajectories within a firework are possible, notably concerning the distribution of velocity $V = |\mathbf{V}|$. In a 3D set of isotropic trajectories uniformly distributed, we know from Maxwell that [34,35]

$$\mathcal{F}(V, n) \sim \frac{V^2}{\langle \mathbf{V}^2 \rangle^{3/2}} e^{-\frac{V^2}{2\langle V^2 \rangle}} \tag{20}$$

is the droplets velocity distribution for a given variance $\langle \mathbf{V}^2 \rangle$ (a function of temperature in gases), depending here on the generation step n, and we have seen that in the Richardson regime $\langle \mathbf{V}^2 \rangle \sim n$, in units of v_0.

At a given maximal cascade step, $0 < n < n_c$, the observed velocity distribution averages over drop trajectories with different ages or step numbers. The drops formed by a mother drop at step n' have further divided themselves a number $n - n'$ of times. Let $\mathcal{N}(n') = e^{\gamma n'}$ be the number of trajectories at step n' (we have $\gamma = \ln 2$ for binary fission), then the velocity distribution averaged over the drop trajectories of the *entire firework* is

$$\mathcal{P}(V) = \int_0^{n_c} \mathcal{N}(n') \mathcal{F}(V, n - n') dn'$$

$$\sim \gamma V e^{-2V\sqrt{\gamma}} \left\{ \text{erfc}\left(\frac{V - n_c \sqrt{\gamma}}{\sqrt{n_c}}\right) \right.$$

$$\left. + e^{4V\sqrt{\gamma}} \text{erfc}\left(\frac{V + n_c \sqrt{\gamma}}{\sqrt{n_c}}\right) \right\}, \tag{21}$$

in agreement, when $\gamma \simeq \ln 4$ and $n_c \simeq 13$ have been properly adjusted, with Fig. 2(d). These values are compatible with our observations and the fact that the number of ejected drops is typically larger but of the order of 2 (see Fig. 1 for example). This completes the study of this original direct (as opposed to inverse [7]) chemically induced capillary cascade architecture, which displays a unique case of a Brownian motion with shrinking steps and also features an accelerated Richardson-like underlying dynamics, two cornerstones of statistical physics, and turbulence.

[1] R. Kraichnan, Inertial ranges in two-dimensional turbulence, Phys. Fluids **10**, 1417 (1967).

[2] A. Alexakis and L. Biferale, Cascades and transitions in turbulent flows, Phys. Rep. **767-769**, 1 (2018).

[3] U. Frisch, *Turbulence: The Legacy of A. N. Kolmogorov* (Cambridge University, Cambridge, England 1995).

[4] B. Dubrulle, Beyond Kolmogorov cascades, J. Fluid Mech. **867**, P1 (2019).

[5] M. P. Brenner, X. D. Shi, and S. R. Nagel, Iterated Instabilities during Droplet Fission, Phys. Rev. Lett. **73**, 3391 (1994).

[6] A. N. Kolmogorov, On the logarithmic normal distribution of particles sizes under grinding, Dokl. Akad. Nauk SSSR **31**, 99 (1941).

[7] E. Villermaux, Fragmentation versus Cohesion, J. Fluid Mech. **898**, P1 (2020).

[8] C. Inoue, Y.-I. Izato, A. Miyake, and E. Villermaux, Direct Self-Sustained Fragmentation Cascade of Reactive Droplets, Phys. Rev. Lett. **118**, 074502 (2017).

[9] N. Bohr, Disintegration of heavy nuclei, Nature (London) **143**, 330 (1939).

[10] K. Pearson, The problem of the random walk, Nature (London) **72**, 294 (1905).

[11] P. L. Krapivsky and S. Redner, Random walk with shrinking steps, Am. J. Phys. **72**, 591 (2004).

[12] L. F. Richardson, Atmospheric diffusion shown on a distance-neighbour graph, Proc. R. Soc. London, Ser. A **110**, 709 (1926).

[13] H. M. De La Rosa Zambrano, G. Verhille, and P. Le Gal, Fragmentation of magnetic particle aggregates in turbulence, Phys. Rev. Fluids **3**, 084605 (2018).

[14] T. B. Oehmke, A. D. Bordoloi, E. Variano, and G. Verhille, Spinning and tumbling of long fibers in isotropic turbulence, Phys. Rev. Fluids **6**, 044610 (2021).

[15] See Supplemental Material at http://link.aps.org/supplemental/10.1103/PhysRevE.104.L053101 for Legend: Movie showing the dynamics of the fragmentation cascade.

[16] L. Landau and E. Lifshitz, *Mechanics*, Course of Theoretical Physics (Elsevier Butterworth-Heinemann, Amsterdam, 1976).

[17] H. Schlichting, *Boundary Layer Theory*, 7th ed. (McGraw-Hill, New York, 1987).

[18] D. Babu, R. J. H. Scanes, R. Plamont, A. Ryabchun, F. Lancia, T. Kudernac, S. P. Fletcher, and N. Katsonis, Acceleration of lipid reproduction by emergence of microscopic motion, Nat. Commun. **12**, 2959 (2021).

[19] G. Quincke, Ueber periodische ausbreitung an flüssigkeitsober-flächen und dadurch hervorgerufene bewegungserscheinungen, Ann. Phys. **271**, 580 (1888).

[20] S. Suda, T. Suda, T. Ohmura, and M. Ichikawa, Straight-To-Curvilinear Motion Transition of a Swimming Droplet Caused by the Susceptibility to Fluctuations, Phys. Rev. Lett. **127**, 088005 (2021).

[21] P. Langevin, Sur la théorie du mouvement brownien, C. R. Acad. Sci. Paris **146**, 530 (1908).

[22] S. Chandrasekhar, Stochastic problems in physics and astronomy, Rev. Mod. Phys. **15**, 1 (1943).

[23] M. Bourgoin, Turbulent pair dispersion as a ballistic cascade phenomenology, J. Fluid Mech. **772**, 678 (2015).

[24] J. Duplat, B. Bossa, and E. Villermaux, On two-dimensional foam aging, J. Fluid Mech. **673**, 147 (2011).

[25] J. Duplat, S. Kheifets, T. Li, M. G. Raizen, and E. Villermaux, Superdiffusive trajectories in Brownian motion, Phys. Rev. E **87**, 020105(R) (2013).

[26] L. S. Ornstein, On the Brownian motion, Proc. Acad. Amsterdam **21**, 96 (1919).

[27] B. Dubrulle, J. P. Laval, and S. Nazarenko, Langevin models of turbulence, in *Progress in Turbulence*, edited by J. Peinke, A. Kittel, S. Barth, and M. Oberlack, Springer Proceedings in Physics Vol. 101 (Springer, Berlin, 2005).

[28] Y. Sumito and K. Yoshikawa, Self-motion of an oil droplet: A simple physicochemical model of active Brownian motion, Chaos **18**, 026106 (2008).

[29] U. Basu, S. N. Majumdar, A. Rosso, and G. Schehr, Active Brownian motion in two dimensions, Phys. Rev. E **98**, 062121 (2018).

[30] J. Yang, M. Davoodianidalik, H. Xia, H. Punzmann, M. Shats, and N. Francois, Passive propulsion in turbulent flows, Phys. Rev. Fluids **4**, 104608 (2019).

[31] L. D. Tambasco, J. J. Pilgram, and J. W. M. Bush, Bouncing droplet dynamics above the Faraday threshold, Chaos **28**, 096107 (2018).

[32] G. J. Janz, Thermodynamic and transport properties for molten salts: Correlation equations for critically evaluated density, surface tension, electrical conductance, and viscosity data, J. Phys. Chem. Ref. Data **17**, 311 (1988).

[33] E. Villermaux, The formation of filamentary structures from molten silicates: Pele's hair, angel hair, and blown clinker, C. R. Mec. **340**, 555 (2012).

[34] J. C. Maxwell, On the dynamical theory of gases, Proc. R. Soc. London **15**, 167 (1867).

[35] W. Pauli, *Thermodynamics and the Kinetic Theory of Gases*, Pauli Lectures on Physics Vol. 3 (Dover, New York, 1973).